The roles of intra-seasonal Kelvin waves and tropical instability waves in SST variability along equatorial Pacific in an isopycnal ocean model

ChuanLi Jiang,* **LuAnne Thompson**

School of Oceanography, University of Washington, Seattle, WA

Kathryn A. Kelly

Applied Physics Laboratory, University of Washington, Seattle, WA

Meghan F. Cronin

NOAA/Pacific Marine Environmental Laboratory, Seattle, WA

December 21, 2008

**Corresponding author address*: ChuanLi Jiang School of Oceanography, Box 357940, University of Washington, Seattle, WA 98195; *e-mail:chuanlij@ocean.washington.edu*

Abstract

The roles of intra-seasonal Kelvin waves and tropical instability waves (TIWs) in the intra-seasonal and low-frequency mixed-layer temperature budget were examined in an isopycnal ocean model forced by QuikSCAT winds from 2000 to 2004. Correlations between temperature tendency and other terms of the intra-seasonal budget compare well with previous results using TAO observations: the net heat flux has the largest correlation in the western Pacific; and zonal advection has the largest correlation in the central Pacific. In the central Pacific, the intra-seasonal variations in zonal advection were due to both the zonal background velocity acting on the Kelvin wave temperature anomaly and the Kelvin wave's anomalous velocity acting on the background temperature. In the eastern Pacific, three of the four temperature budget terms have comparable correlations. In particular, the vertical processes acting on the shallow thermocline cause large SST anomalies in phase with the intra-seasonal thermocline anomalies.

On intra-seasonal time scales, the influence of composite upwelling and downwelling Kelvin waves cancel each other. However, because the intra-seasonal SST anomalies increase to the east, a zonal gradient of SST is generated that is in phase with intra-seasonal zonal velocity. Consequently, heat advection by the Kelvin waves rectifies into lower frequencies in the eastern Pacific. Rectification due to TIWs was also seen. The prevalence of intra-seasonal Kelvin waves and the zonal structure of intra-seasonal SST from 2002 to early 2004 suggested that they might be important in setting the eastern Pacific SST on interannual time scales.

1. Introduction

Previous research suggests possible connections between intra-seasonal downwelling Kelvin waves driven by westerly wind bursts in the western Pacific and the SST warming in the eastern Pacific on both intra-seasonal and low frequency time scales (Harrison and Schopf 1984; Harrison and Giese 1988; Giese and Harrison 1991; Kessler et al. 1995; McPhaden 1999; Kessler and Kleeman 2000; Vecchi and Harrison 2000; Zhang and Gottschalck 2002; McPhaden 2002; Kutsuwada and McPhaden 2002; Seo and Xue 2005). On intra-seasonal time scales, the downwelling Kelvin waves can remotely affect the eastern Pacific SST by changing the zonal current structure in the central and eastern equatorial Pacific (Harrison and Giese 1988; Giese and Harrison 1991; Kessler et al. 1995; Vecchi and Harrison 2000), by changing the thermocline slope (Zhang 2001), and by influencing the meridional advection by the tropical instability waves (TIWs) (Giese and Harrison 1991). See Kessler (2005) for a review. Intra-seasonal signal can also rectify into lower frequencies through nonlinearities. In the western Pacific, Kessler and Kleeman (2000) found rectification in SST by the feedback between the warm pool SST and Madden-Julian Oscillation (MJO). Likewise, if the intra-seasonal wave causes temperature gradient anomalies that are in phase with the velocity anomalies, then advective processes can cause the anomalies to rectify into lower frequencies. For instance, Jochum and Murtugudde (2004) found rectification in SST from TIWs in the eastern Pacific.

McPhaden (2002) examined the physical processes that control the intra-seasonal SST variability in the equatorial Pacific at four TAO (Tropical Atmospheric-Ocean) moorings sites (165^oE, 170^oW, 140^oW, and 110^oW). McPhaden found that zonal advection dominates in the central Pacific and vertical advection and entrainment dominate in the eastern Pacific. His findings provided an explanation for the warming and cooling events that occurred simultaneously over a wide longitude range, as noted by Kessler and McPhaden (1995) during the 1991/1992 El Niño. McPhaden argued that the increased importance of vertical advection and entrainment in the eastern Pacific, which leads the thermocline depth by a quarter of cycle, can cause the SST to vary in phase along the equator or even to appear to propagate westward. We note that if SST varied in phase perfectly with the same magnitude at all longitudes, then there would be no zonal SST gradient anomalies associated with Kelvin waves and the temperature advection would not rectify into lower frequencies. Likewise, if the SST anomaly was perfectly in phase with the velocity anomaly, then the zonal SST gradient due to the wave would be zero exactly when the velocity anomaly was maximum and, again, there would be no rectification into lower frequencies. Given the complexity of the dynamics in the equatorial Pacific and the approximation and assumptions invoked by the empirical analysis, it is not clear that these two cases are uniformly valid. In this study we will use a numerical model to investigate the intra-seasonal variations due to Kelvin waves and whether and how advection rectifies intra-seasonal variations into the lower frequency temperature balance. We also will examine potential rectification by tropical instability waves.

Legeckis (1977) first characterized TIWs from satellite sea surface temperature (SST), with a period of about 25 days and a wavelength of about 1000 km. The contribution of TIWs to the low frequency SST anomalies in the eastern Pacific, particularly to seasonal SST anomalies, has been studied in the past (Hansen and Paul 1984; Swenson and Hansen 1999; Wang and McPhaden 1999; Kessler et al. 1998; Polito et al. 2001; Menkes et al. 2006; Jochum and Murtugudde 2004). Many of these studies emphasize the role of TIWs in warming the cold tongue in its seasonal evolution through horizontal eddy heat transport. Determining how TIWs modulate both intra-seasonal and low frequency SST anomalies of the cold tongue in an OGCM with improved forcing of high-resolution QuikSCAT winds is the secondary goal of this study.

The overall goal of this study is to explore the influence of horizontal advection by Kelvin waves and TIWs on both the intra-seasonal and low frequency SST variability in the equatorial Pacific. The improved high-resolution satellite forcing enables us to investigate this influence with more realism than was possible before. The QuikSCAT winds have been shown to provide high accuracy and high resolution winds that produce more realistic mean SST, 20^oC isotherm depth, and latent heat flux than NCEP reanalysis-2 winds (Jiang et al. 2008). They also provide high quality hybrid turbulent heat fluxes in the tropical Pacific (Jiang et al. 2005; Zhang 2006). Thus QuikSCAT winds would be expected to allow an ocean model to accurately simulate intra-seasonal Kelvin waves and TIW variability, along with their SST response.

The model and data used in this study are described in Section 2. Section 3 gives a detailed comparison between the model and the observations. The mixed-layer temperature budget analysis on both the intra-seasonal and low-frequency time scales are described in Section 4 and Section 5, respectively. The roles of the intra-seasonal Kelvin waves and the tropical instability waves in the horizontal advection and influence on the temperature budgets are also examined. Finally, we give a discussion and summary in Section 6.

2. Model and data

The GFDL Hallberg Isopycnal Model (HIM, Hallberg (1997); Ladd and Thompson (2002)) was used in this study. HIM is a three-dimensional, isopycnal coordinate, C-grid general ocean circulation model. A Kraus-Turner-like bulk mixed layer which is similar to the Kraus-Turner model except that the contribution to the entrainment velocity by wind mixing decays with mixed-layer depth, and Richardson number dependant mixing are implemented in the model (Oberhuber

1993). Note that the mixed layer is one single model layer. The model domain extended from $100^oE - 70^oW$, $30^oS - 30^oN$ in the tropical Pacific, with 1^o in longitude and 0.5^o in latitude, and 16 layers in the vertical including an active mixed layer. The biharmonic along-isopycnal viscosity (9 $\times$ 10^{11} m^4/s) is used. A biharmonic form of Smagorinsky's nonlinear eddy viscosity is also used, with the nondimensional biharmonic Smagorinsky's constant 0.032. The kinematic viscosity below the mixed layer is 1 $\times$ 10^{-4} m^2/s. For the diffusivity, the along-isopycnal tracer diffusivity is 1 $\times$ 10^3 m^2/s, and the diapycnal diffusivity of density below the mixed layer is 3 $\times$ 10^{-5} m^2/s. We spun up the model for 10 years using ECMWF (European Centre for Medium-Range Weather Forecasts) 40-yr Reanalysis (ERA40) forcing from January 1995 to December 1999 repeated once, and then we ran the model for five years from January 2000 to December 2004 using QuikSCAT winds, ISCCP (International Satellite Cloud Climatology Project) shortwave and longwave radiation, and NCEP reanalysis-2 (NCEP2) for other atmospheric state variables.

It has been shown that QuikSCAT winds have smaller errors than NWP (Numerical Weather Prediction) reanalysis winds when compared to TAO buoy winds (Kelly et al. 1999; Chelton et al. 2001; Jiang et al. 2005). The model was forced by the 1^o $\times$ 1^o gridded daily QuikSCAT winds field (Kelly et al. 1999). For the shortwave and longwave radiation, we chose 1^o $\times$ 1^o daily ISCCP data. The turbulent heat fluxes (latent and sensible heat fluxes) were calculated in the model using the University of Arizona bulk algorithm (Zeng et al. 1998) from QuikSCAT wind speed, NCEP2 reanalysis atmospheric variables, and model SST. Single variables (e.g.,T, u, v, etc) and mixed-layer temperature budget terms from January 2000 to December 2004 were saved as five-day averaged fields for analysis. See Jiang et al. (2008) for details on the dynamical forcing fields used in this study.

To gain confidence in the analysis, the model SST and 20^oC isotherm depth (Z20) averaged between 2^oS and 2^oN are compared with TAO array buoy measurements within $2^oS - 2^o$N. We also compare the model SST along 2^oN with the fusion SST product from Remote Sensing Systems (RSS), which is an optimally interpolated SST map using TMI Tropical Rainfall Measuring Mission (TRMM) Microwave Imager) sensor.

To obtain the intra-seasonal signal, which is primarily Kelvin waves but also includes some energy from Rossby waves propagating from the far eastern Pacific, we used a bandpass scheme similar to that used in McPhaden (2002). The five-year mean and seasonal cycle were first subtracted from the initial time series to derive an anomalous time series. The anomalous time series were then low-pass filtered with a filter whose half-power frequency was 30 days and another filter whose half-power frequency was 90 days. The bandpassed intra-seasonal signal was the difference between the above two low-pass filtered results. The time series associated with tropical instability waves (hereafter called high-frequency) was obtained by high-pass filtering the anomalous time series with a filter whose half-power frequency was 30 days. The above bandpass scheme with intra-seasonal Kelvin waves and TIWs is justified by the distinct peak gaps between 20^oC isotherm depth at 0^o140^oW and SST at 2^oN125^oW for both the observations and the model (Fig. 1). A peak of 50$-$75 days (Kelvin waves) is shown in TAO Z20 at 0^o140^oW, and a peak of 20$-$35 days (TIWs) is shown in TMI SST at 2^oN125^oW. The respective values for the model match well with the observations. Note that the peaks in both the observations and the model are statistically significant.

[Figure 1 about here.]

3. Comparison of the model with observations

The model compares well with mean TAO measurements along the equator (Fig. 2) in most aspects (Jiang et al. 2008). The five-year-mean temperature from the model (Fig. 2c) matches well with the TAO observations (Fig. 2a) for isotherms above 15^oC, but is much colder below. Additionally, the mean model temperature in the eastern Pacific (around 110^oW) is slightly warmer than the observations above 200m. The mean zonal velocity from the model (Fig. 2d) captured the main features of the observed velocity (Fig. 2b), with the maximum magnitude of the equatorial undercurrent (EUC) in the model only slightly weaker and the position of the EUC core only slightly deeper than observed. The weak EUC in the model might be partly responsible for the slightly warm temperature in the eastern Pacific. The westward ocean currents in the western Pacific shown in the observations was not simulated well in the model, probably owing to either the poor data availability of TAO observations or the coarse coastline and topography used in the model there.

The time-longitude plots of Z20 and SST in the model agree well with TAO measurements (not shown). The model Z20 is slightly shallower in the western Pacific and deeper in the east. Consistent with errors in Z20, the model SST is slightly colder in the western equatorial Pacific, and warmer in the eastern equatorial Pacific than observed. The time series of model Z20 correlates well with the observations in the central and eastern Pacific (c $\geq$ 0.60), while the correlation is relatively small in the western Pacific around 160^oE. For SST, the model and the observations correlate well in the central and eastern Pacific (c$>$0.75), but not as well in the western Pacific. The poor data availability of TAO observations and the coarse coastline and topography used in the model are two possible factors that contribute to the small correlations in the western Pacific.

[Figure 2 about here.]

3a. *Intra-seasonal*

The intra-seasonal signal in the model, as represented by Z20, compares well with the observations, especially in phase speed (Fig. 3a, c). The eastward propagation of Z20 can be seen in both the observations and the model and is associated with the propagation of downwelling and upwelling Kelvin waves, generated in response to both westerly wind bursts and easterly wind anomalies in the western Pacific. The magnitude of the intra-seasonal thermocline fluctuation (up to 20m) in the model is generally larger than in the observation, which suggests that the intra-seasonal Kelvin waves in the model are somewhat too vigorous. The time-longitude plots of the intra-seasonal sea surface temperature also compare well with the TMI observations (Fig. 3b, d). Contrary to the eastward propagation of the Z20, the warming and cooling events on intra-seasonal timescales occurred near simultaneously over a wide range of longitudes or even appeared to propagate westward, especially in the eastern Pacific. This phenomena has also been noticed in the 1990s and early 2000s (Kessler and McPhaden 1995; Zhang 2001; McPhaden 2002). Note that the magnitude of the SST variations tended to increase from west to east. As a result, the zonal gradient of the intra-seasonal temperature showed large magnitude in the eastern Pacific, which can be seen in both the observations and the model (Fig. 4a, b). The intra-seasonal zonal velocity anomalies propagate eastward in phase with Z20 anomalies (Fig. 4c). However, an interesting pulsing pattern can also be seen in the zonal velocity that we interpret as interference between eastward propagating Kelvin and westward propagating Rossby waves. It is noteworthy that the magnitude of the zonal velocity by the Kelvin wave is much larger than that of the Rossby wave. The effect of this interference pattern is westward propagating zonal convergence anomalies that appear to be responsible for the westward propagation of the intra-seasonal zonal temperature gradient anomalies shown in Fig. 4 a and b.

[Figure 3 about here.]

[Figure 4 about here.]

The intra-seasonal Z20 time series in the model correlates well with TAO in the central Pacific (c $\geq$ 0.60). The correlations are relatively low, however, in the far western and eastern Pacific, which might be due to the too vigorous Kelvin waves there in the model. For the intra-seasonal SST, the model agrees well with the observations in the western and central Pacific, but has a relatively small correlation in the eastern Pacific (not shown).

3b. *High frequency*

The 30$-$day high-pass filtered SST in the model (Fig. 5a) agrees well with TMI SST (Fig. 5b) along $2^o N$. The westward propagation of the TIWs can be easily seen, especially during autumn and winter. The model did not capture very well TIW activity in the central Pacific in the second half of 2000 and 2001. However, the model simulated well the strong TIW activity in early 2003, whose importance will be addressed in detail later.

[Figure 5 about here.]

The strength of TIWs in the model, which can be illustrated by the meridional velocity (time averaged from January 2000 to December 2004) in the mixed layer at $0^o 140^o W$, is consistent with the meridional velocity observations of TAO array at 35m depth, which is in the middle of the mixed layer in the model (Fig. 2). In addition, the meridional velocity in the mixed layer at

0^o140^oW has a period of approximately 20 days, which is consistent with the peak in the velocity at 35m depth from 0^o140^oW TAO mooring (not shown). The five-year TAO time series at 140^oW and 110^oW along the equator show a surface (35m) maximum of EKE (eddy kinetic energy) of 436 cm^2/s^2 and 649 cm^2/s^2 with periods less than 30 days, the respective values for the model are 403 cm^2/s^2 and 562 cm^2/s^2.

4. Intra-seasonal mixed-layer temperature budget

Given the adequate performance of the model in reproducing the variability and the mean along the equator mentioned in Section 3, we proceed with the budget analysis to investigate the roles of Kelvin waves and TIWs in SST variability.

The mixed-layer temperature (MLT) in the model evolves in a sequential manner with the following five steps: (1) horizontal advection, (2) horizontal diffusion, (3) net surface heat flux, (4) vertical diffusion, and (5) entrainment. We calculate the mixed-layer temperature budget terms associated with each of these processes by evaluating the temperature values before and after the relevant model routines are recorded (Dawe and Thompson 2007). The MLT budget closes and is consistent with the representation of the temperature budget in the model. The vertical diffusion is not separated from the vertical entrainment term in this study. The horizontal diffusivity term is much smaller (averaged $\sim 0.1^oC\ yr^{-1}$) than other terms ($\sim 1 - 10^oC\ yr^{-1}$) so that it is excluded in the analysis. At the same time as the temperature is evolved in the model, the mixed-layer depth and other layer thickness also evolve, such that the mixed-layer depth at each step and the model temperature evolution are consistent.

Thus the four primary mixed-layer temperature budget terms that influence its tendency ($\frac{\partial T}{\partial t}$)

are the zonal advection, meridional advection, vertical diffusion and entrainment, and the net surface heat flux absorbed in the mixed layer (absorbed shortwave radiation in the mixed layer, net outgoing longwave radiation, sensible heat flux, and latent heat flux) respectively. For a shorthand, we write those four terms as $-u\frac{\partial T}{\partial x}$, $-v\frac{\partial T}{\partial y}$, $-w_e\frac{\triangle T}{h}$, and $\frac{Q_{net}}{\rho_0 C_p h}$, with u, v, and w_e being the mixed-layer zonal velocity, meridional velocity, and vertical entrainment at the base of the mixed layer, ρ_0 the seawater density, C_p the heat capacity, h the mixed-layer depth, and $\triangle T$ the temperature difference between the mixed layer and the temperature of the layer being entrained into the mixed layer. Q_{net} in this study represents the net surface heat flux absorbed in the mixed layer, and is equivalent to the adjusted net surface heat flux Q_{adj} used in McPhaden (2002). We emphasize, however, that as discussed earlier, our method of estimating these terms differs from that typically used in empirical analyses such as McPhaden (2002). In particular, each term, including vertical diffusion and entrainment, is calculated implicitly at each model time step.

4a. *Along the equator*

The correlations between the intra-seasonal MLT tendency and each of the other four temperature budget terms along the equator are shown in the left panel of Fig. 6. The correlations on the same four TAO moorings as in McPhaden (2002) are presented in the right panel of Fig. 6 to facilitate the comparison with his results. The time series of the model at a certain mooring location are obtained by taking the mean of the nearby model points within 5^o longitude. The model suggested an important role for zonal advection (top panel) at all longitudes on the equator, with the largest correlations in the central Pacific. The net surface heat flux term (bottom panel) has the largest correlation in the western Pacific. In the eastern Pacific, zonal advection, vertical diffusion and entrainment, and the meridional advection all have comparable magnitudes of correlations with the temperature tendency. The net heat flux has the smallest correlation in the eastern Pacific, especially east of 120^oW. In general, the model results at the four TAO sites (right panel of Fig. 6) compare well with those of McPhaden (2002) (his figures 6, 8, 10,and 12) that were based on TAO buoy data at those four sites: the correlation between the zonal advection and the temperature tendency is largest in the central Pacific, and the correlation between the net surface heat flux and temperature tendency is the largest in the western Pacific. However, in the eastern Pacific the model differs from his result: three of those four terms (zonal advection, vertical diffusion and entrainment, and meridional advection) have comparable magnitudes, whereas McPhaden found that the vertical flux and entrainment dominated. It is noteworthy that the vertical term in McPhaden (2002) is the residual of other budget terms. The model result suggested that, when following a single Kelvin wave, one would expect to see the effect of zonal advection from the wave on the intra-seasonal temperature tendency in the central Pacific, but not necessarily in the eastern Pacific since other two other processes contribute as well.

[Figure 6 about here.]

To determine which physical processes associated with Kelvin waves and TIWs contribute most to the temperature tendency along the equator, we decomposed the zonal and meridional advection terms by frequency. We independently bandpass filtered the temperature and velocities, and then calculated the contribution to the tendency from each crossterm. We decomposed each single variable (e.g., T, u, v) into three parts: high frequency, which represents the TIWs (*hf*, $<$ 30 days), intra-seasonal signal, which represents primarily the Kelvin waves, but also includes other variability such as from Rossby waves generated in the far eastern Pacific (*is*, 30 days $-$ 90 days), and the residual signal, which we hearafter refer to as the low-frequency signal (*lf*, $>$ 90 days). The residual low-frequency signal includes the seasonal cycle, the interannual signal and the five-year mean.

Single variables can be expressed as a sum of three frequency band components:

$$
\begin{aligned}
T &= T_{hf} + T_{is} + T_{lf}; \\
u &= u_{hf} + u_{is} + u_{lf}; \\
v &= v_{hf} + v_{is} + v_{lf};
\end{aligned}
\tag{1}
$$

Their contribution to the advection gives 9 crossterms for zonal advection:

$$
\begin{aligned}
u\frac{\partial T}{\partial x} &= (u_{hf} + u_{is} + u_{lf}) \times \frac{\partial}{\partial x}(T_{hf} + T_{is} + T_{lf}) \\
&= u_{hf}\frac{\partial T_{hf}}{\partial x} + u_{hf}\frac{\partial T_{is}}{\partial x} + u_{hf}\frac{\partial T_{lf}}{\partial x} \\
&+ u_{is}\frac{\partial T_{hf}}{\partial x} + u_{is}\frac{\partial T_{is}}{\partial x} + u_{is}\frac{\partial T_{lf}}{\partial x} \\
&+ u_{lf}\frac{\partial T_{hf}}{\partial x} + u_{lf}\frac{\partial T_{is}}{\partial x} + u_{lf}\frac{\partial T_{lf}}{\partial x},
\end{aligned}
\tag{2}
$$

and meridional advection:

$$
\begin{aligned}
v\frac{\partial T}{\partial y} &= (v_{hf} + v_{is} + v_{lf}) \times \frac{\partial}{\partial y}(T_{hf} + T_{is} + T_{lf}) \\
&= v_{hf}\frac{\partial T_{hf}}{\partial y} + v_{hf}\frac{\partial T_{is}}{\partial y} + v_{hf}\frac{\partial T_{lf}}{\partial y} \\
&+ v_{is}\frac{\partial T_{hf}}{\partial y} + v_{is}\frac{\partial T_{is}}{\partial y} + v_{is}\frac{\partial T_{lf}}{\partial y} \\
&+ v_{lf}\frac{\partial T_{hf}}{\partial y} + v_{lf}\frac{\partial T_{is}}{\partial y} + v_{lf}\frac{\partial T_{lf}}{\partial y}
\end{aligned}
\tag{3}
$$

We calculated each term separately from filtered five-day averaged variables and then filtered the crossterms to determine how much each contributed to the temperature tendency in the corresponding frequency band (hf, is, and lf). The physical interpretation of some crossterms in (2) and (3) are listed in Table 1.

[Table 1 about here.]

We first examine the zonal advection contribution to the intra-seasonal temperature tendency. In the central Pacific, where the correlation with temperature tendency is largest, intra-seasonal zonal advection is owing both to advection of intra-seasonal temperature gradient by the low-frequency zonal velocity ($-u_{lf}\frac{\partial T_{is}}{\partial x}$, Table 1 (a)) and advection of the low-frequency temperature gradient by the intra-seasonal zonal velocity ($-u_{is}\frac{\partial T_{lf}}{\partial x}$, Table 1 (b)). This implies that the intra-seasonal waves can affect the temperature in the central Pacific by both modifying the zonal current structure (u_{is}) and the zonal temperature gradient ($\frac{\partial T_{is}}{\partial x}$). In the eastern Pacific, $-u_{lf}\frac{\partial T_{is}}{\partial x}$ increases and dominates, owing to the larger anomalous zonal temperature gradient there (Fig. 4b). As discussed earlier, the increased magnitude of the intra-seasonal SST anomaly in the eastern Pacific results in an anomalous zonal SST gradient.

The contribution to the intra-seasonal temperature tendency from meridional advection crossterms (Fig. 7b) is relatively small when compared to zonal advection (Fig. 7a). However, among the 9 crossterms in (3), there are two terms that stand out in the eastern Pacific: meridional advection of the mean temperature gradient by the intra-seasonal meridional velocity $-v_{is}\frac{\partial T_{lf}}{\partial y}$, which might be owing to cross-equatorial wind stress anomalies, and the high-frequency nonlinear term $-v_{hf}\frac{\partial T_{hf}}{\partial y}$ (Table 1 (e)) produced by the TIWs that rectify into the intra-seasonal band.

[Figure 7 about here.]

One might argue that if the largest crossterms in either zonal or meridional advection could cancel, then their sum would not matter to the intra-seasonal temperature tendency. However, the largest crossterms, averaged from 150^oW to 90^oW, are not significantly anticorrelated, and thus they appear to play a role in the intra-seasonal temperature tendency.

4b. *Along the composite Kelvin waves*

The intra-seasonal signal in this study includes primarily the Kelvin waves, but also includes some energy from intra-seasonal Rossby waves in the far eastern Pacific. Therefore, to examine the effect of intra-seasonal Kelvin waves on SST variability, it is important to quantify how much a composite downwelling or upwelling Kelvin wave contributes to the intra-seasonal SST anomaly at a certain location. From the contours of the intra-seasonal time-longitude plots of the 20^oC isotherm depth along the equator ($2^oS - 2^oN$), we tracked 14 downwelling (dark dotted lines in Fig. 3c) and 12 upwelling (white dotted lines in Fig. 3c) Kelvin waves during the five-year period. For each downwelling Kelvin wave, for instance, we determined its temporal and spatial extent from the positive maximum anomaly of the intra-seasonal 20^oC isotherm depth. Note that Z20 is positive throughout this paper. The temporal and spatial locations of all 14 downwelling and 12 upwelling Kelvin waves for single variables (e.g., T, u, v, etc) and mixed-layer temperature budget terms were then obtained. Finally, at each longitude grid point, we averaged the single variables and budget terms over periods of anomalous positive and negative Z20 to obtain the average values for respectively downwelling and upwelling Kelvin waves.

As evident in Fig. 8, there was a warming anomaly almost all the way from west to east along the trajectory of a composite downwelling Kelvin wave. In the central Pacific, from 180^o to 125^oW, zonal advection along the composite downwelling Kelvin wave accounted for most of the positive anomaly in the temperature tendency (Fig. 8a). In the eastern Pacific, east of 130^oW, however, the vertical diffusion and entrainment started to play an important role (Fig. 8b). The region separation of those two processes appeared to be much less than $2,500Km$, a quarter of the Kelvin wavelength. Thus, the time for a composite Kelvin wave to travel from the region where the zonal advection dominates to the region where the vertical processes contribute is short relative to the time for SST to respond to zonal advection. Therefore, warming by a single downwelling Kelvin wave could occur earlier in the eastern than in the central Pacific, given the fact that the vertical diffusion and entrainment leads the zonal advection by a quarter of cycle. It is noteworthy that the magnitude of the meridional advection along Kelvin waves (not shown) is smaller than the zonal advection, and vertical diffusion and entrainment.

We also found apparent cancellations of the temperature tendency, zonal advection, vertical diffusion and entrainment along the equator between the composite downwelling and upwelling Kelvin waves. Zonal advection and vertical processes tend to oppose the cooling anomalies by an upwelling Kelvin wave, although this cancellation is not exact. As shown in the histograms of the intra-seasonal Z20 along 14 downwelling (Fig. 8c) and 12 upwelling (Fig. 8d) Kelvin waves, the mean magnitude of Z20 along the two selected types of waves are the same (about $12m$).

[Figure 8 about here.]

5. Low-frequency mixed-layer temperature budget

For the low-frequency temperature budget ($>$90 days), the correlation results are similar to those of the intra-seasonal time scale: zonal advection has a significant correlation with temperature tendency along the equator, especially in the central Pacific (Fig. 9 top panel). In addition, the net surface heat flux (Fig. 9 bottom panel) has the largest correlation with temperature tendency in the western Pacific. Meridional advection and vertical diffusion and entrainment have slightly smaller correlations along the equator than zonal advection and net surface heat flux, but might still be important.

[Figure 9 about here.]

Of the three crossterms in (2) that contribute significantly to the low-frequency zonal advection, advection of the low-frequency temperature gradient by the low-frequency velocity ($-u_{lf}\frac{\partial T_{lf}}{\partial x}$, Table 1 (c)) has the largest magnitude (Fig. 10a). This term is associated with the interaction between the low-frequency horizontal velocity with temperature gradient fluctuations. The rectification from the intra-seasonal Kelvin waves ($-u_{is}\frac{\partial T_{is}}{\partial x}$, Table 1 (d)) is associated with the interaction between the intra-seasonal zonal current with zonal SST gradient by the intra-seasonal waves to the temperature tendency and contributes significantly in the eastern Pacific. In addition, there is a small rectification from tropical instability waves ($-u_{hf}\frac{\partial T_{hf}}{\partial x}$). There are no significant anticorrelations between the largest crossterms, suggesting that they are all crucial terms in zonal advection (Fig. 11a, b). Whether or not those crossterms contribute greatly to the low-frequency temperature tendency requires a complete decomposition analysis of all the budget terms, including the vertical diffusion and entrainment and net heat flux, which can not be easily done using the same bandpass method as in the horizontal advection, because the mixed layer depth evolves in concert with other variables in this isopycnal model. The time series of the largest crossterms in zonal advection (Fig. 11a), averaged from 150^oW to 90^0W, suggest that the rectification from intra-seasonal waves ($-u_{is}\frac{\partial T_{is}}{\partial x}$) is a positive (warming) contribution to the low-frequency temperature tendency from late 2002 to early 2004.

[Figure 10 about here.]

For meridional advection, rectification from tropical instability waves ($-v_{hf}\frac{\partial T_{hf}}{\partial y}$, Table 1 (e)) has the largest magnitude from 140^oW to 110^oW among all the crossterms (Fig. 10b). As in the zonal advection, there are no significant cancellations between the largest crossterms in the meridional advection (Fig. 11b). The term associated with the interaction between the low-frequency meridional velocity and temperature gradient fluctuations ($-v_{lf}\frac{\partial T_{lf}}{\partial y}$) showed seasonal cycles, with cooling in March and warming in September. Meanwhile, the cooling by this term in early 2003 seems to be mostly compensated by the anomalous warming by the rectification from TIWs ($-v_{hf}\frac{\partial T_{hf}}{\partial y}$), indicating a possibly important role of TIWs in the seasonal evolution of the cold tongue.

[Figure 11 about here.]

It can be shown that the approaches used by Kessler and Kleeman (2000) and Shinoda and Hendon (2002) to calculate the rectification are comparable to the bandpassed method used in this study. Briefly, the rectification from an anomalous signal ($V^{'}$) to the mean (V_{mean}) in their approaches is the running mean of the difference between a product of the anomalous signals plus their means and a product of the means. In analogy to their approach, the rectification in the zonal advection is defined as the running mean of the difference between the following two terms: $(u_{mean}+u_{is})\frac{\partial(T_{mean}+T_{is})}{\partial x}$ and $u_{mean}\frac{\partial(T_{mean})}{\partial x}$. The signal longer than 90 days was referred to as the "mean" in Shinoda and Hendon (2002), and is the same as the low-frequency signal in this study. Therefore, the rectification using their approaches before the 90-day running mean is identical to three crossterms in this study ($u_{is}\frac{\partial T_{is}}{\partial x}$, $u_{is}\frac{\partial T_{lf}}{\partial x}$, and $u_{lf}\frac{\partial T_{is}}{\partial x}$). We found that rectification calculated from their approaches is primarily from one single bandpass filtered term ($u_{is}\frac{\partial T_{is}}{\partial x}$) in this study.

The low-frequency temperature tendency has both seasonal and interannual cycles (Fig.12a), while the rectification of the intra-seasonal waves occurred during the second year of 2002, the whole year of 2003, and the first half of 2004 (Fig. 12b). The large magnitude of the rectification was mainly centered in the eastern Pacific, especially east of 140^oW, where large magnitude of the zonal gradient of the intra-seasonal SST was found (Fig. 4). As mentioned in Section 4, the increased magnitude of the intra-seasonal temperature tendency in the east by the Kelvin waves (Fig. 8) might be responsible for the large SST gradient, and therefore the rectification. Five years of analysis is not long enough to identify which timescale of temperature tendency the intra-seasonal Kelvin waves rectified to. Meanwhile, there is distinct rectification of the tropical instability waves in the meridional advection term in early 2003, which might be associated with the strong TIW activity during that period, as shown in Fig. 5. This strong TIW activity caused a large positive latitudinal SST gradient (over $1^oC/$ between 2^oN and equator); the resulting warming of the cold tongue may have contributed to the demise of the 2003 La Ni$\tilde{n}$a (McPhaden 2004). It is yet unclear whether this strong TIW activity is related to the prevalence of intra-seasonal Kelvin waves from 2002 to 2004.

[Figure 12 about here.]

6. Discussion and conclusion

In this study, we examined the contribution of Kelvin waves and TIWs to the intra-seasonal and low-frequency mixed-layer temperature tendency from 2000 to 2004. An isopycnal ocean model was forced with QuikSCAT winds, ISCCP shortwave and longwave radiation, and other NCEP2 meteorological variables.

The model captured well the mean and variability along the equator compared to observations. The intra-seasonal variability of Z20, the SST and its zonal gradient compared well with TAO observations. The zonal SST gradient has large magnitude in the eastern Pacific and appeared to propagate westward in the far east. The intra-seasonal anomalies in the zonal SST gradient are ultimately caused by the large SST variations to the east caused by vertical processes acting on the shallow thermocline there. These large SST variations tend to be in phase with weaker SST variations in the central Pacific and thus result in a SST zonal gradient. Once this gradient is generated, the westward propagating zonal convergence associated with the Kelvin and Rossby wave interference pattern causes the zonal temperature gradient to also propagate westward. Additionally, the TIW signals along $2^o N$ in the model agreed well with the TMI SST observations, especially in early 2003. The strength of TIWs in the model is consistent with the TAO observations.

The intra-seasonal mixed-layer temperature budget is consistent with the results of McPhaden (2002) based on four TAO moorings: the temperature tendency has the largest correlation with the net surface heat flux in the western Pacific, where the thermocline is deep; and with zonal advection in the central Pacific. In the eastern Pacific, the model differs from McPhaden's results, in that three of the four temperature budget terms (zonal advection, vertical diffusion and entrainment, and meridional advection) have comparable correlations with temperature tendency. In particular, the vertical processes acting on the shallow thermocline cause large SST anomalies in phase with the intra-seasonal thermocline anomalies.

The intra-seasonal temperature budget analysis along the composite Kelvin wave confirmed the above results along the equator. The region where the zonal advection dominates was found to be adjacent and to the east of the region where the vertical processes contribute, with the transition occurring roughly at 130^oW. This finding can not be achieved from TAO observations because of their sparse resolution (McPhaden 2002; Zhang 2001). Meanwhile, this finding confirms the statement of McPhaden (2002) that the growing importance of the vertical diffusion and entrainment in the eastern Pacific is responsible for the in-phase or even westward propagating SST variations shown in Fig. 3. Furthermore, there were apparent cancellations in the intra-seasonal temperature tendency, zonal advection, and vertical diffusion and entrainment between the composite downwelling and upwelling Kelvin waves. These cancellations suggested that the importance of Kelvin waves to SST variability depends on the ratio of the numbers of downwelling to upwelling Kelvin waves weighted by their strength and only the linear effect is considered.

We decomposed the horizontal advection terms into three spectral bands (high-frequency: $<$30 days; intra-seasonal: 30 days$-$90 days; low-frequency: $>$90 days). For the intra-seasonal temperature tendency, a comparison of the contributions suggested that zonal advection of the intra-seasonal temperature gradient by the low-frequency zonal velocity $-u_{lf}\frac{\partial T_{is}}{\partial x}$ and zonal advection of the low-frequency temperature gradient by intra-seasonal zonal velocity $-u_{is}\frac{\partial T_{lf}}{\partial x}$ are comparable in the central Pacific, but that $-u_{lf}\frac{\partial T_{is}}{\partial x}$ dominates in the eastern Pacific where the thermocline is shallow. A small contribution from the meridional advection of the high-frequency meridional temperature gradient by high-frequency meridional velocity, $-v_{hf}\frac{\partial T_{hf}}{\partial y}$, indicated a rectification of meridional advection from the TIWs to the intra-seasonal temperature tendency.

The low-frequency mixed-layer temperature tendency has the largest correlation with zonal advection in the central Pacific, and with the net surface heat flux in the western Pacific, but all budget terms might contribute to low-frequency temperature tendency in the eastern Pacific.

We found rectification in horizontal advection from the intra-seasonal waves and TIWs to be secondary contributors, with the largest contribution from the advection of the low-frequency temperature gradients by low-frequency velocities. The rectification from the intra-seasonal waves ($-u_{is}\frac{\partial T_{is}}{\partial x}$) had large magnitude in the eastern Pacific, especially east of 140^oW, where large magnitude of the zonal gradient of the intra-seasonal SST can also be found. In addition, the cancellations we found in the intra-seasonal temperature tendency between a composite downwelling and upwelling Kelvin wave does not indicate there would be no net contribution. There would be no net contribution from a downwelling Kelvin wave and a subsequent upwelling Kelvin wave only in a linear context, in which no interaction among intra-seasonal oscillations (for instance $-u_{is}\frac{\partial T_{is}}{\partial x}$) occurred. It is the nonlinearity between the intra-seasonal zonal velocity and the zonal gradient of the intra-seasonal SST by the Kelvin waves that resulted in the rectification to low-frequency SST. The rectification in SST by the feedback between the warm pool SST and MJO in the western Pacific has been found in Kessler and Kleeman (2000). This study, however, provided the physical mechanism for the rectification in SST from intra-seasonal waves in the eastern Pacific.

The rectification in SST from TIWs in the eastern Pacific has been found in the coupled model of Jochum et al. (2007b) and Jochum and Murtugudde (2004). This study suggested that the strong TIW activity associated with strong SST fronts along 2^oN and cold SST on the equator in early 2003 may be responsible for the rectification of the TIWs to the low-frequency temperature tendency. Averaged from $150^oW - 90^oW$, the magnitude of the rectification of TIWs in early 2003 to the low-frequency SST variability is comparable with the cooling contribution from low-frequency interaction. This implies that anomalously strong TIWs in early 2003 warm the cold tongue, which may contribute to the abrupt cessation of the La Ni$\tilde{n}$a in early 2003 (McPhaden 2004).

Since we only decomposed the horizontal advection terms in this study, the rectification from the intra-seasonal Kelvin waves and TIWs to the low-frequency temperature tendency through zonal advection might be smaller than other MLT budget terms and therefore have less of a contribution to the low-frequency temperature tendency. Further and more complete studies are required to determine the roles of these two types of waves to the low-frequency SST variability. Meanwhile, the low-frequency analysis in this study includes both the seasonal cycle and the interannual variability, our results did not indicate the exact time scales on which the Kelvin waves and TIWs rectified. With only five years of QuikSCAT wind forcing, we could not examine the longer time scale in detail. It would be interesting to explore further this scale interaction when a longer period of QuikSCAT winds is available. In addition, our analysis focused on the equatorial temperature budget, not on the meridional temperature structure. Using a numerical model, Jochum and Murtugudde (2006) showed that the off-equatorial zonal heat flux convergences by the TIWs were comparable in size to the meridional eddy heat flux convergence on the equator. This was verified by Jochum et al. (2007a) using on and off-equatorial current meter measurements. According to Jochum and Murtugudde (2006), TIWs act as a vertical heat pump and increase the net air-sea surface heat flux on the annual-mean time scale. Further temperature budget studies with longer model runs are needed to determine whether or not the rectification from intra-seasonal Kelvin waves and TIWs are critical to ENSO and to climate variability.

Acknowledgement The authors would like to thank Suzanne Dickinson for preparing the QuikSCAT gridded winds and NCEP2 fields. We would also like to thank Jordan T. Dawe and David Darr for their help in HIM model. NCEP2 reanalysis data are obtained from ftp://ftp.cdc.noaa.gov/Datasets/-ncep.reanalysis2.dailyavgs/. ECMWF ERA40 data have been obtained from http://data.ecmwf.int/data/d/era40_daily/. The TAO buoy data are from NOAA's Pacific Marine Environmental Laboratory (PMEL) http://www.pmel.noaa.gov/tao/data_deliv/. We also acknowledge the TAO Project Office, Dr. Michael J. McPhaden, Director. This work was supported by grant GC99-370 from the NOAA Office of Global Programs Pan American Climate Studies, and NASA's Ocean Vector Winds Science Team through contract 1285662 with the Jet Propulsion Laboratory.

References

Chelton, D., S. Esbensen, M. Schlax, N. Thum, and M. Freilich, 2001: Observations of coupling between surface wind stress and sea surface temperature in the eastern tropical Pacific. *J. Climate*, **14**, 1479–1498.

Dawe, J. and L. Thompson, 2007: PDO-related heat and temperature budget changes in a model of the north Pacific. *J. Climate*, **20**, 2092–2108.

Giese, B. and D. Harrison, 1991: Eastern equatorial Pacific response to three composite westerly wind types. *J. Geophys. Res.*, **96**, 3239–3248.

Hallberg, R., 1997: Localized coupling between surface and bottom intensified flow over topography. *J. Phys. Oceanogr.*, **27**, 27 911–27 988.

Hansen, D. V. and C. A. Paul, 1984: Genesis and effects of long waves in the equatorial Pacific. *J. Geophys. Res.*, **89**, 10,430–10,440.

Harrison, D. and B. Giese, 1988: Remote westerly wind forcing of the eastern equatorial Pacific: some model results. *Geophys. Res. Lett.*, **15**, 804–807.

Harrison, D. and P. Schopf, 1984: Kelvin-wave-induced anomalous advection and the onset of surface warming in El Niño events. *Mon. Wea. Rev.*, **112**, 923–933.

Jiang, C., M. F. Cronin, K. Kelly, and L. Thompson, 2005: Evaluation of a hybrid satellite- and NWP-based turbulent heat flux product using Tropical Atmosphere-Ocean (TAO) buoys. *J. Geophys. Res.*, **110**, C09007.

Jiang, C., L. Thompson, and K. Kelly, 2008: Equatorial influence of QuikSCAT winds in an isopycnal ocean model compared to NCEP2 winds. *Ocean Modeling*, 10.1016/j.ocemod.2008.05.003.

Jochum, M., M. F. Cronin, W. S. Kessler, and D. Shea, 2007a: Observed horizontal temperature advection by Tropical Instability Waves. *Geophys. Res. Lett.*, **34**, doi:10.1029/2007GL029416.

Jochum, M., C. Deser, and A. Phillips, 2007b: Tropical atmospheric variability forced by oceanic internal variability. *J. Climate.*, **20**, 765–771.

Jochum, M. and R. Murtugudde, 2004: Internal variability in the tropical Pacific ocean. *Geophys. Res. Lett.*, **31**, doi:10.1029/2004GL020488.

— 2006: Temperature advection by tropical instability waves. *J. Phys. Oceanogr.*, **36**, 592–605.

Kelly, K., S. Dickinson, and Z.-J. Yu, 1999: NSCAT tropical wind stress maps: Implications for improving ocean modeling. *J. Geophys. Res.*, **105**, 11 291–11 310.

Kessler, W. and R. Kleeman, 2000: Rectification of the Madden Julian Oscillation into the ENSO cycle. *J. Climate*, **13**, 3560–3575.

Kessler, W. and M. McPhaden, 1995: 1991-93 El Niño in the central Pacific. *Deep-Sea Res.*, **42B**, 295–334.

Kessler, W., M. McPhaden, and K. Weickman, 1995: Forcing of intraseasonal Kelvin waves in the equatorial Pacific. *J. Geophys. Res.*, **100**, 10 613–10 631.

Kessler, W., L. Rothstein, and D. Chen, 1998: The annual cycle of SST in the eastern tropical Pacific, diagnosed in an ocean GCM∗. *J. Climate*, **11**, 777–799.

Kessler, W. S., 2005: Intraseasonal variability in the oceans. *Intraseasonal variability of the Atmosphere-Ocean system.*, W.K.M Lau and D.E. Waliser, Eds. Praxis Publishing.

Kutsuwada, K. and M. McPhaden, 2002: Intraseasonal variations in the upper equatorial Pacific Ocean prior to and during the 1997-98 El Niño. *J. Phys.Oceanogr.*, **32**, 1133–1149.

Ladd, C. and L. Thompson, 2002: Decadal variability of north Pacific central mode water. *J. Phys. Oceanogr.*, **32**, 2870–2881.

Legeckis, R., 1977: Long waves in the eastern equatorial Pacific ocean - A view from a geostationary satellite. *Science*, **197**, 1179–1181.

McPhaden, M., 1999: Genesis and evolution of the 1997-98 El Niño. *Science*, **283**, 950–954.

— 2002: Mixed layer temperature balance on intraseasonal time scales in the equatorial Pacific Ocean. *J. Climate*, **15**, 2632–2647.

— 2004: Evolution of the 2002-03 El Niño. *Bull. Amer. Meteor. Soc.*, **85**, 677–695.

Menkes, C., V. JG., K. SC., J. Boulanger, and M. GV., 2006: A modeling study of the impact of tropical instability waves on the heat budget of the eastern equatorial Pacific. *J. Phy. Oceanogr.*, **36**, 847–865.

Oberhuber, J., 1993: Simulation of the Atlantic circulation with a coupled sea ice-mixed layer-isopycnal general circulation model. Part I: Model description. *J. Phys. Oceanogr.*, **23**, 808–829.

Polito, P., J. Ryan, W. Liu, and P. Chavez, 2001: Oceanic and atmospheric anomalies of tropical instability waves. *Geophys. Res. Lett.*, **28**, 2233–2236.

Seo, K.-H. and Y. Xue, 2005: MJO-related oceanic Kelvin waves and the ENSO cycle: A study with the NCEP Global Ocean Data Assimilation System. *Geophys. Res. Lett.*, **32**, L07712.

Shinoda, T. and H. H. Hendon, 2002: Rectified wind forcing and latent heat flux produced by the Madden-Julian Oscillation. *J. Climate*, **15**, 3500–3508.

Swenson, M. and D. Hansen, 1999: Tropical Pacific ocean mixed layer heat budget: the Pacific cold tongue. *J. Phys. Oceanogr.*, **29**, 69–81.

Vecchi, G. and D. Harrison, 2000: Tropical Pacific sea surface temperature anomalies, El Niño, and Equatorial westernly wind events. *J. Climate*, **13**, 1814–1830.

Wang, W. and M. J. McPhaden, 1999: The surface-layer heat balance in the equatorial Pacific Ocean. Part I: mean seasonal cycle. *J. Phys. Oceanogr.*, **29**, 1812–1831.

Zeng, X., M. Zhao, and R. E. Dickinson, 1998: Intercomparison of bulk aerodynamic algorithms for the computation of sea surface fluxes using TOGA COARE and TAO data. *J. Climate*, **11**, 2628–2644.

Zhang, C., 2001: Intraseasonal perturbations in Sea Surface Temperature of the Equatorial eastern Pacific and their association with the Madden-Julian Oscillation. *J. Climate*, **14**, 1309–1322.

— 2006: The impact of satellite winds and latent heat fluxes in a numerical simulation of the Tropical Pacific Ocean. *J. Climate*, **19**, 5889–5902.

Zhang, C. and J. Gottschalck, 2002: SST anomalies of ENSO and the Madden-Julian Oscillation in the equatorial Pacific. *J. Climate*, **15**, 2429–2445.

List of Figures

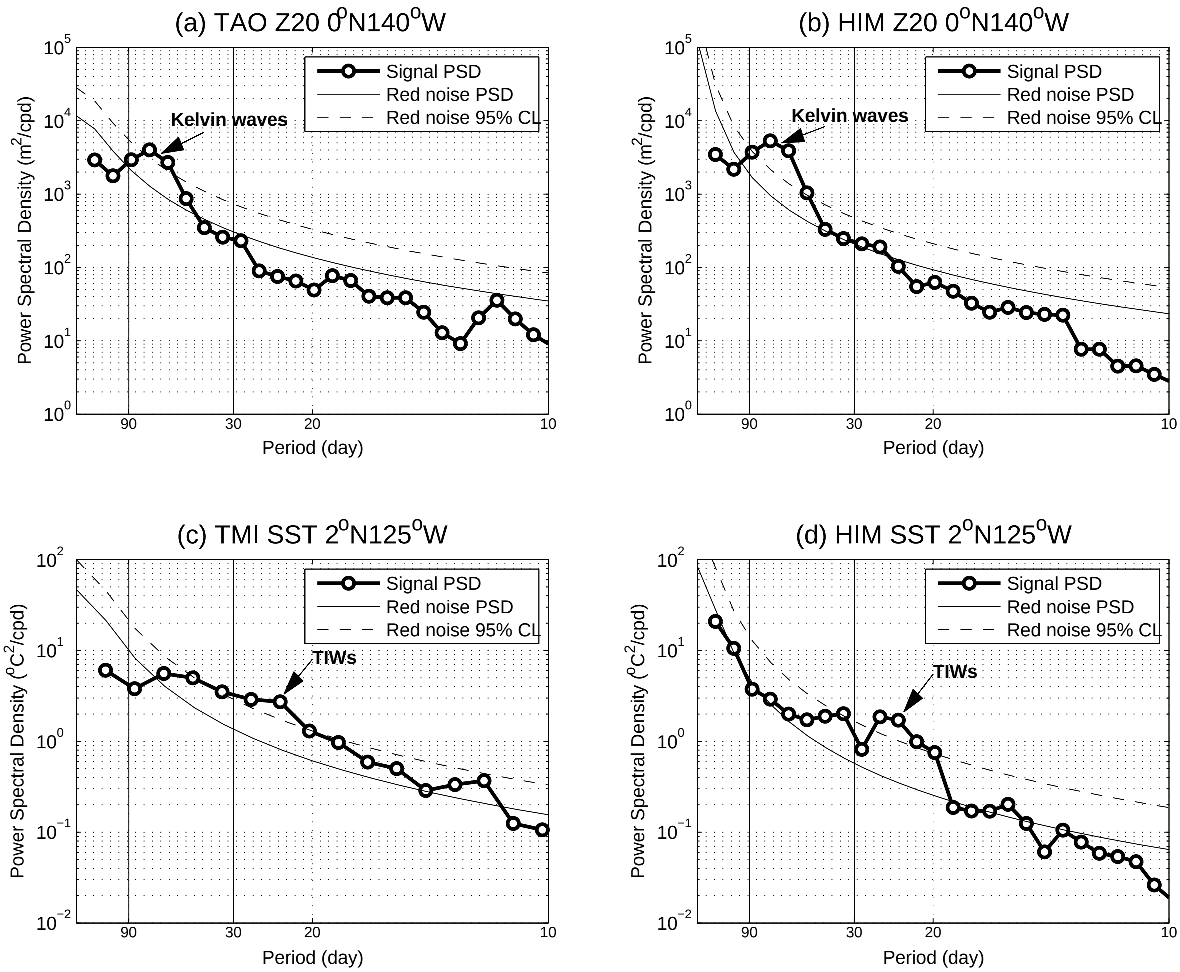

Figure 1: Power spectral density of Z20 (m) at 0^oN140^oW where the distinct signal of Kelvin waves were shown for (a) TAO, and (b) HIM; and power spectral density of SST (^oC) at 2^oN125^oW where the distinct signals of TIWs were shown for (c) TAO, and (d) HIM. The smooth solid curve is the spectrum of red noise which has the same total variance as the signal. The dashed curve is the 95% confidence level (CL) needed to reject a null hypothesis of red noise on a priori basis.

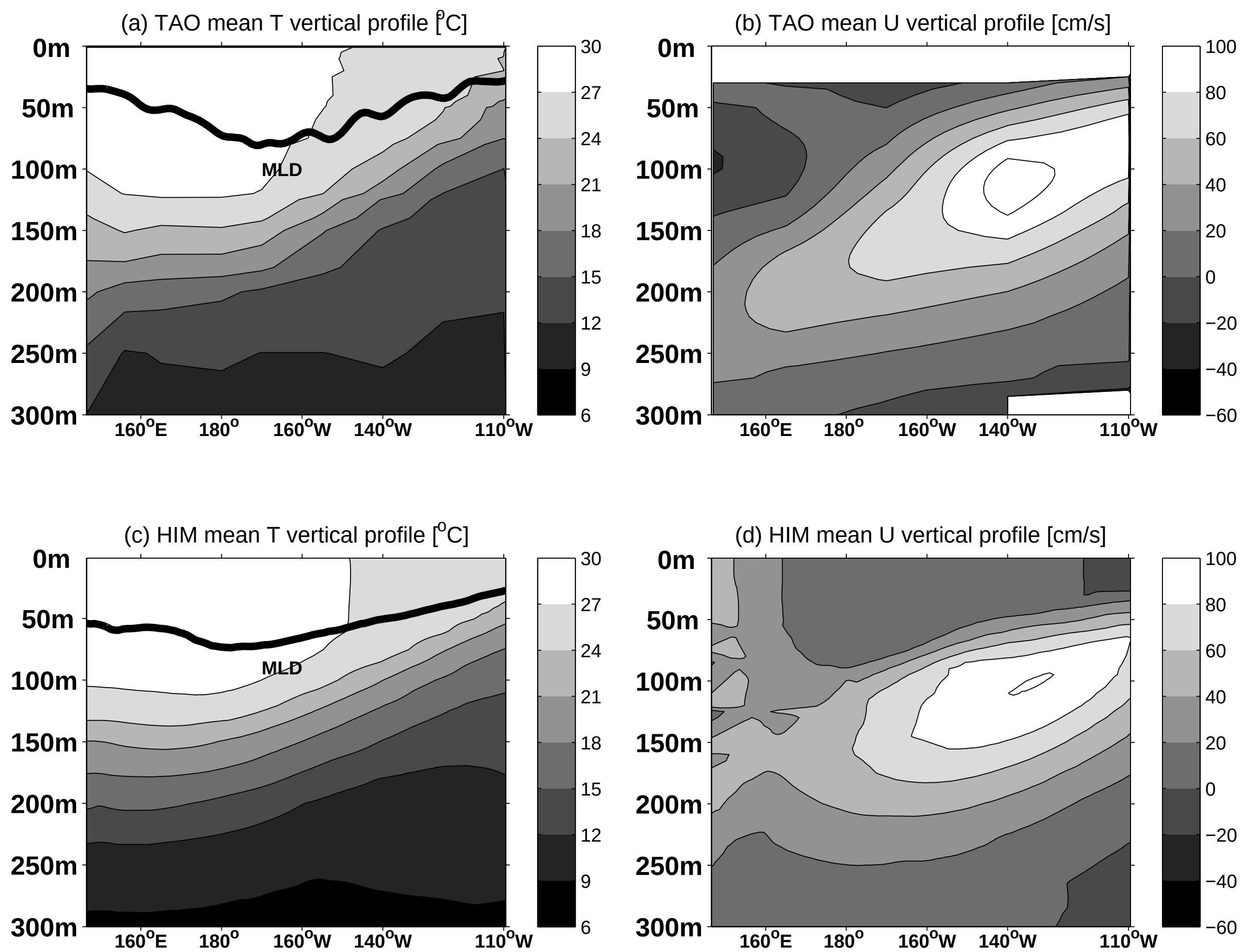

Figure 2: Five-year-mean temperature (^oC) (left panel) and zonal velocity (cm/s) (right panel) from TAO (upper panel) and from the model (lower panel) along the equator (averaged over $2^oS - 2^oN$). The dark black line in (a) shows the mean Levitus mixed layer depth, and the dark black line in (c) shows the mean mixed layer depth in the model.

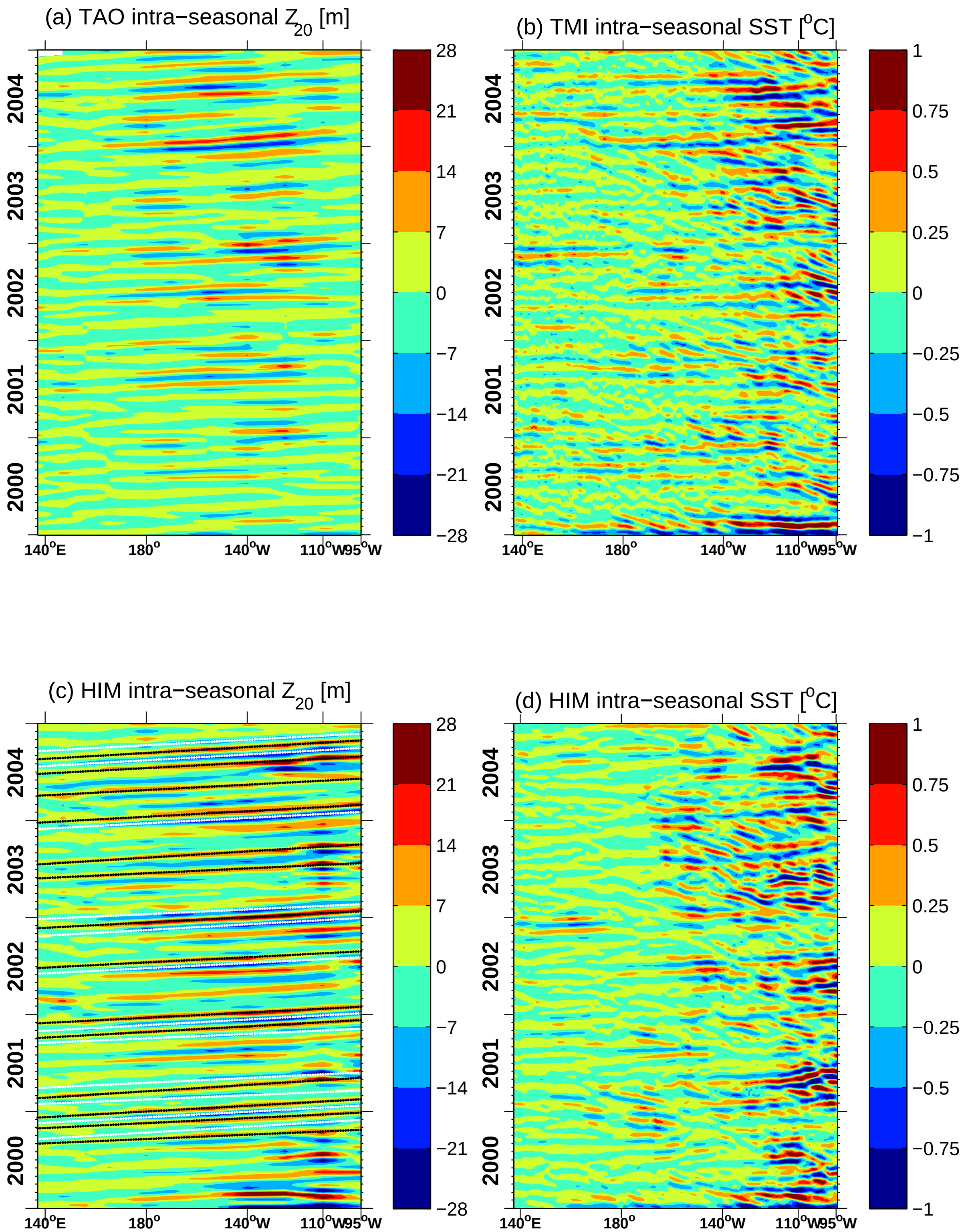

Figure 3: Time-longitude plots of the intra-seasonal (a) TAO 20^oC isotherm depth, (b) TMI SST, (c) HIM 20^oC isotherm depth, and (d) HIM SST. The 14 dotted black lines in (c) show the selected downwelling Kelvin wave ray paths, and the 12 dotted white lines show the upwelling Kelvin wave ray paths. The zonal grid resolutions in (b) and (d) are 1 degree.

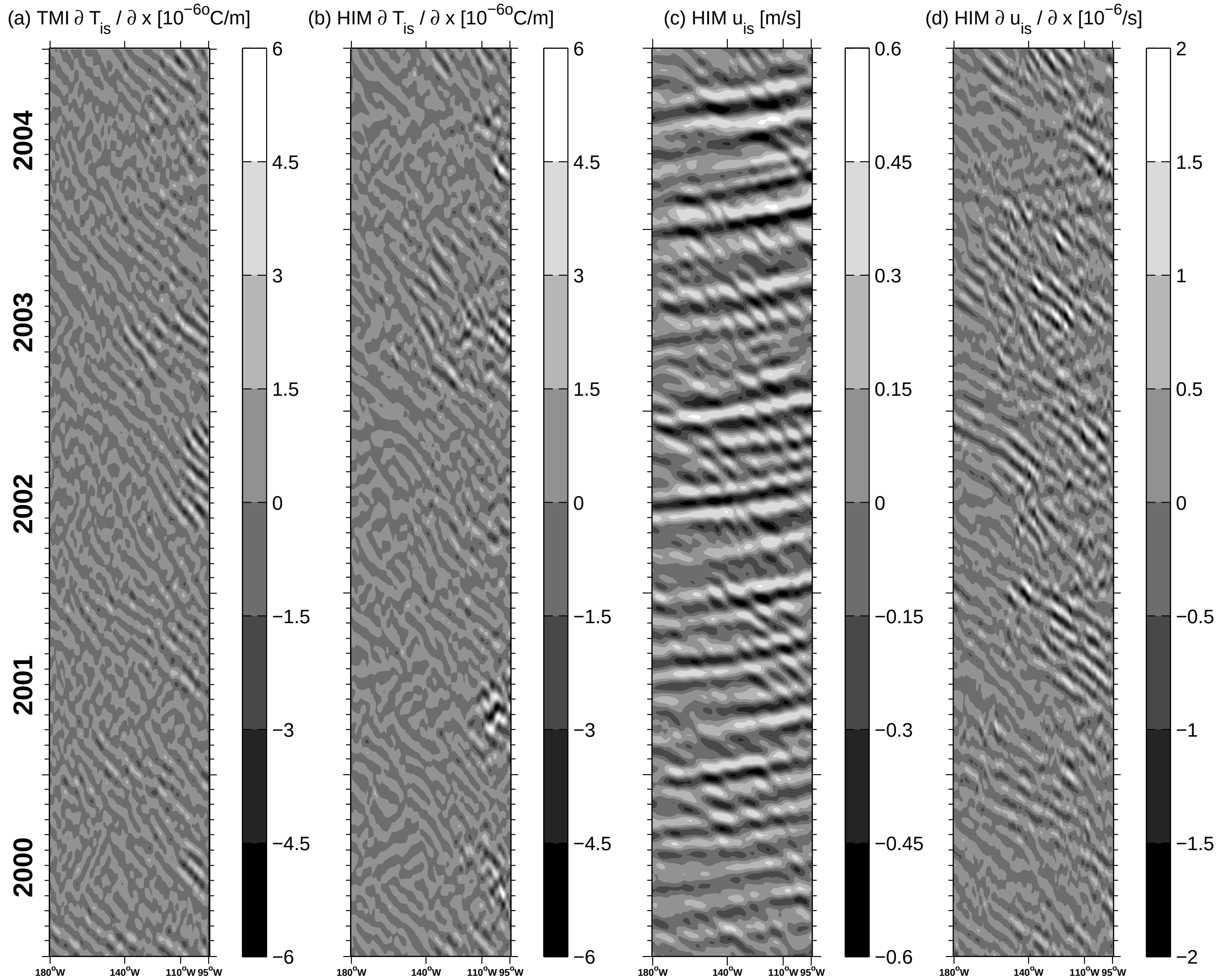

Figure 4: Time-longitude plots of the equatorial (a) TMI $\partial T_{is}/\partial x$, (b) HIM $\partial T_{is}/\partial x$, (c) HIM zonal velocity u_{is}, and (d) HIM $\partial u_{is}/\partial x$.

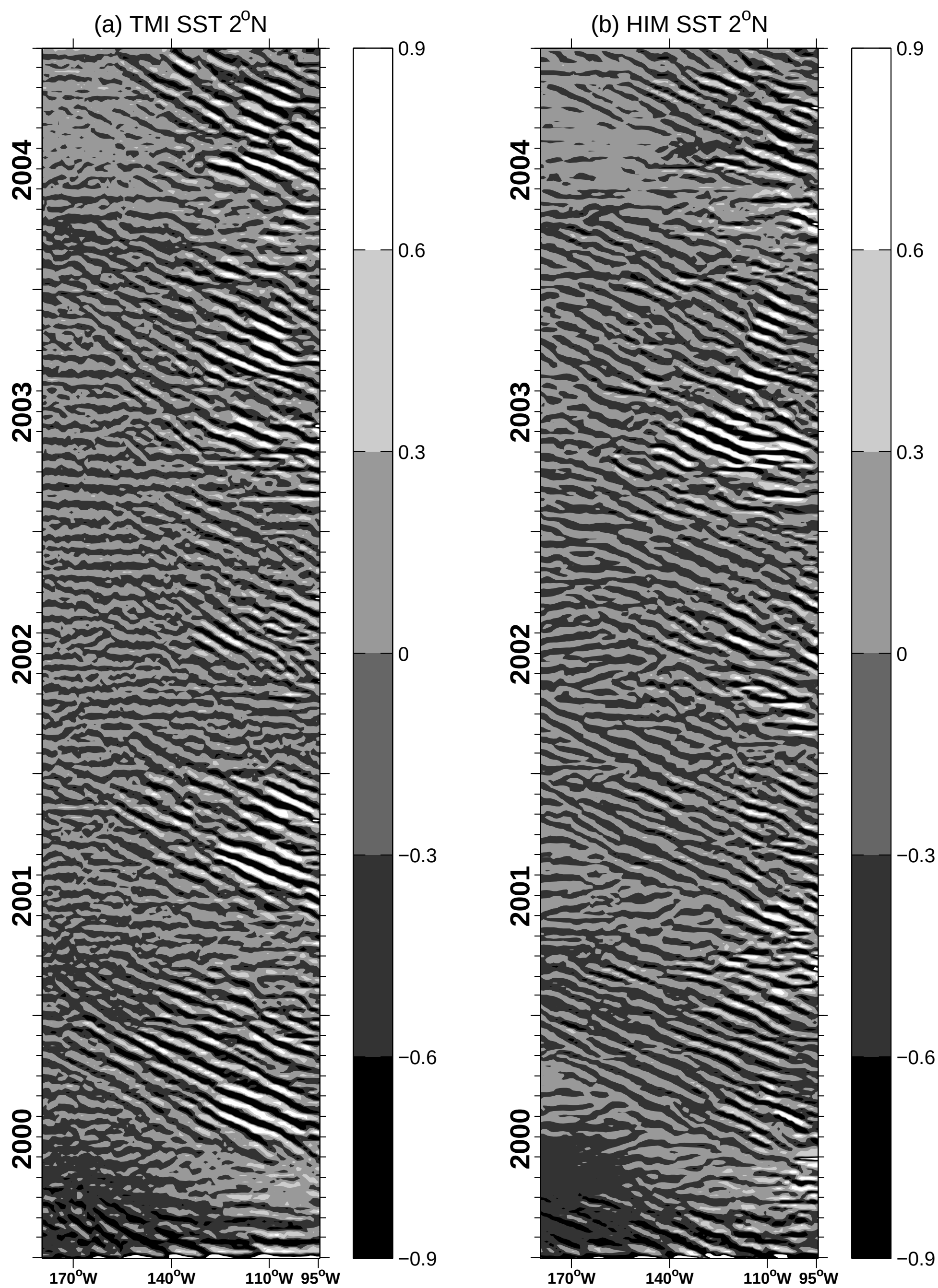

Figure 5: Time-longitude plots of the 30-day highpassed SST (^{o}C) along 2^{o}N for (a) TMI, and (b) the model.

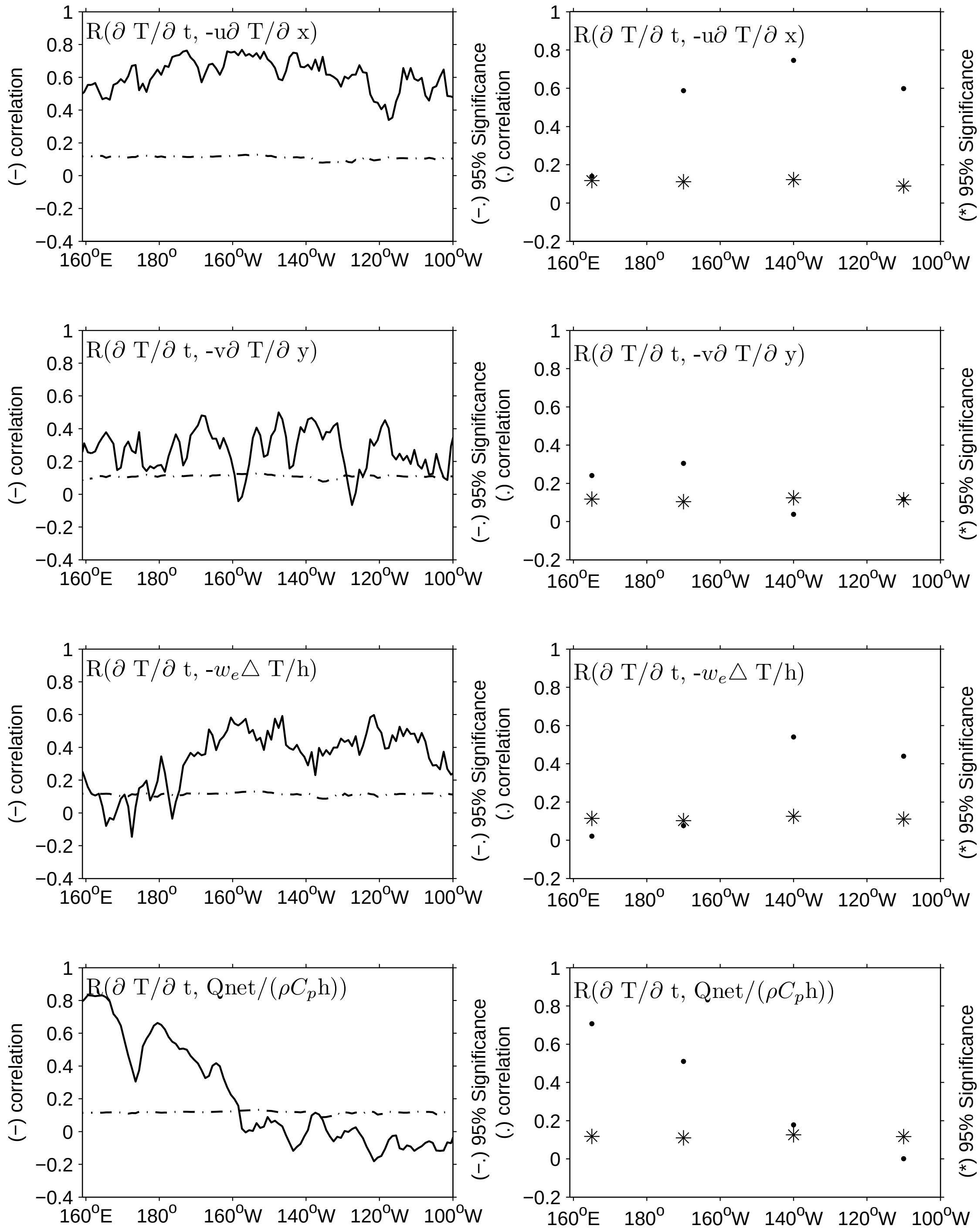

Figure 6: Correlations of the intra-seasonal temperature tendency with temperature budget terms: zonal advection, meridional advection, vertical diffusion and entrainment, and net surface heat flux (from top to bottom, left panel) along the equator. Corresponding values at four TAO buoys are shown in the right panel. Ninety-five percent confidence limits for the correlations (dash-dot lines in left panel, asterisks in right panel) are also shown.

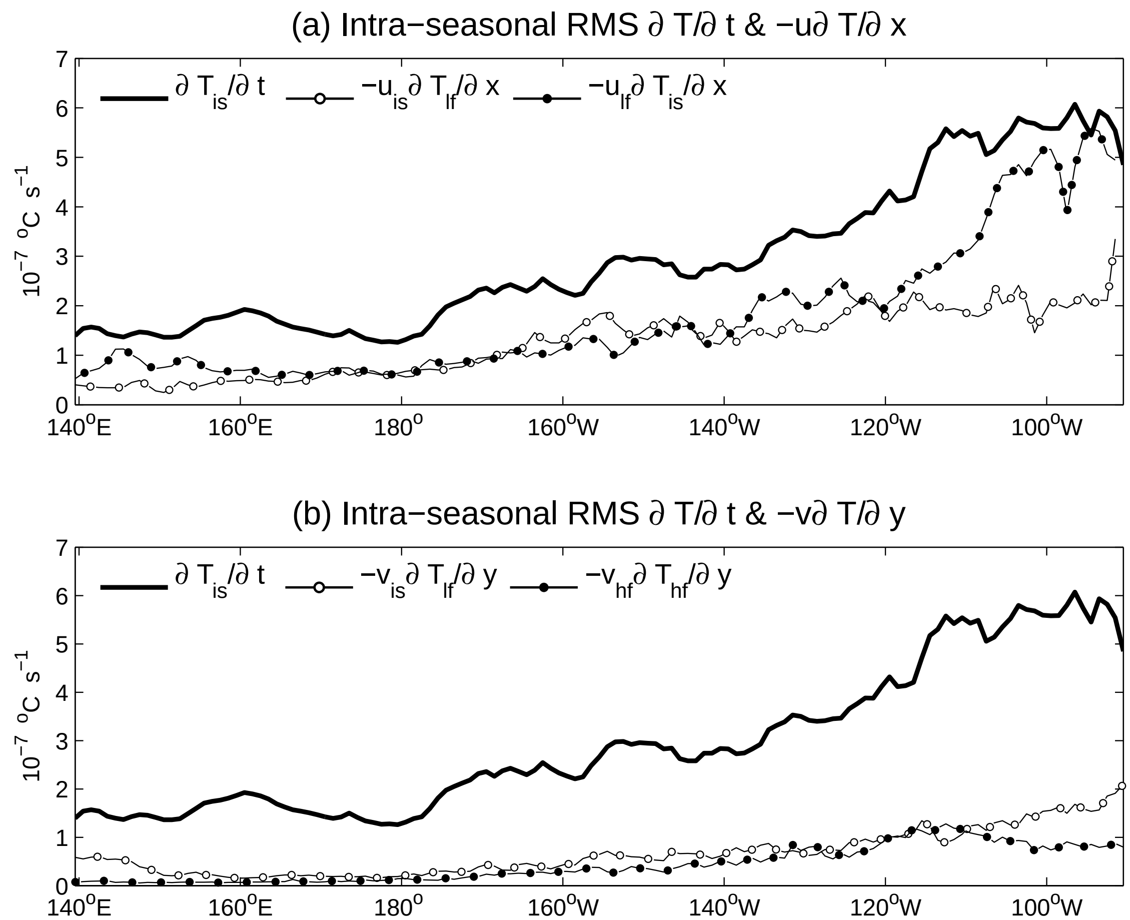

Figure 7: Root mean square (RMS) of the intra-seasonal temperature tendency and the decompositions of (a) the zonal advection, and (b) the meridional advection along the equator.

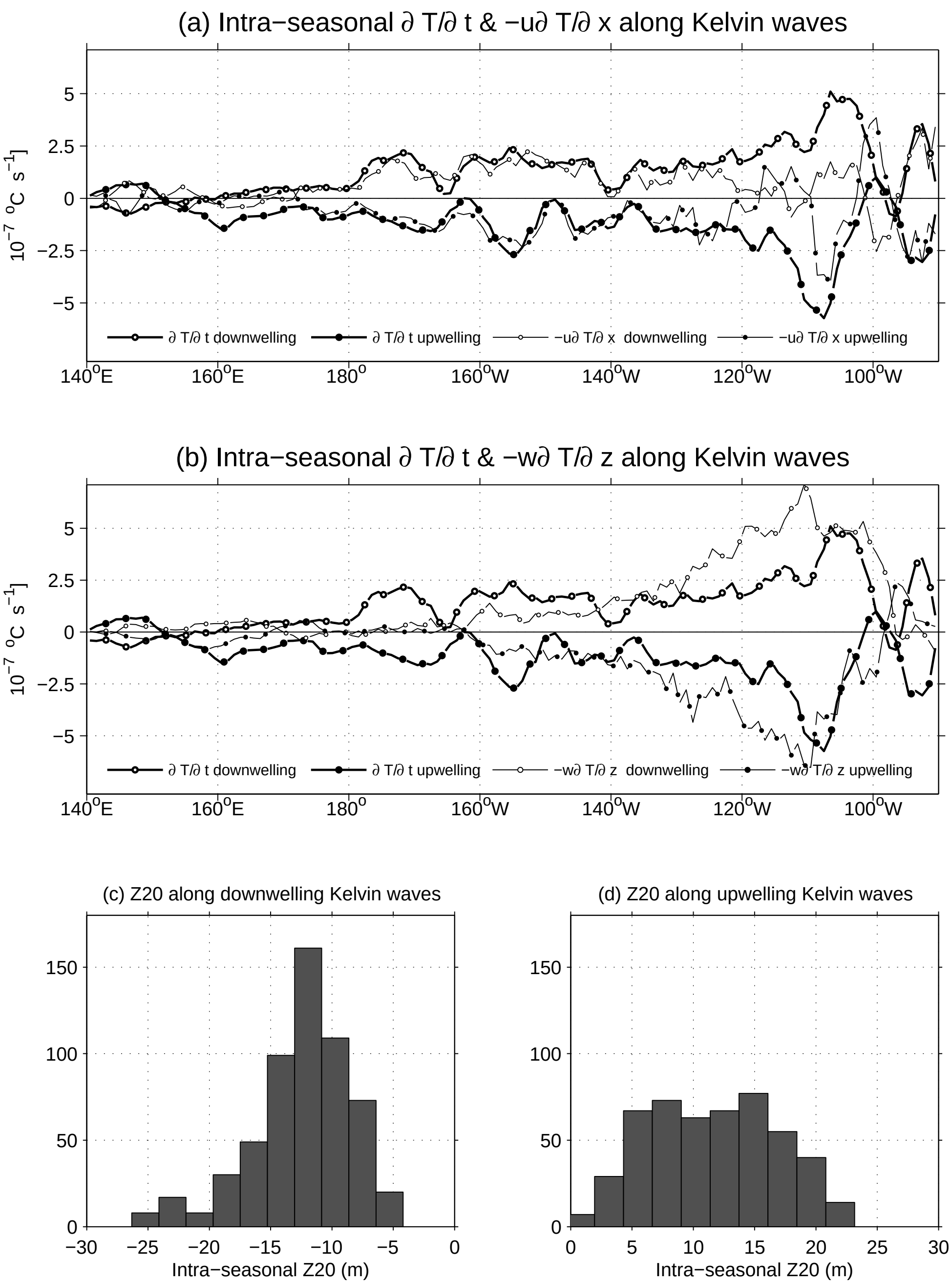

Figure 8: (a) The intra-seasonal temperature tendency versus zonal advection along composite Kelvin waves, (b) temperature tendency versus vertical diffusion and entrainment along composite Kelvin waves, (c) histogram of the intra-seasonal Z20 for all 14 downwelling Kelvin waves, and (d) histogram of the intra-seasonal Z20 for all 12 upwelling Kelvin waves.

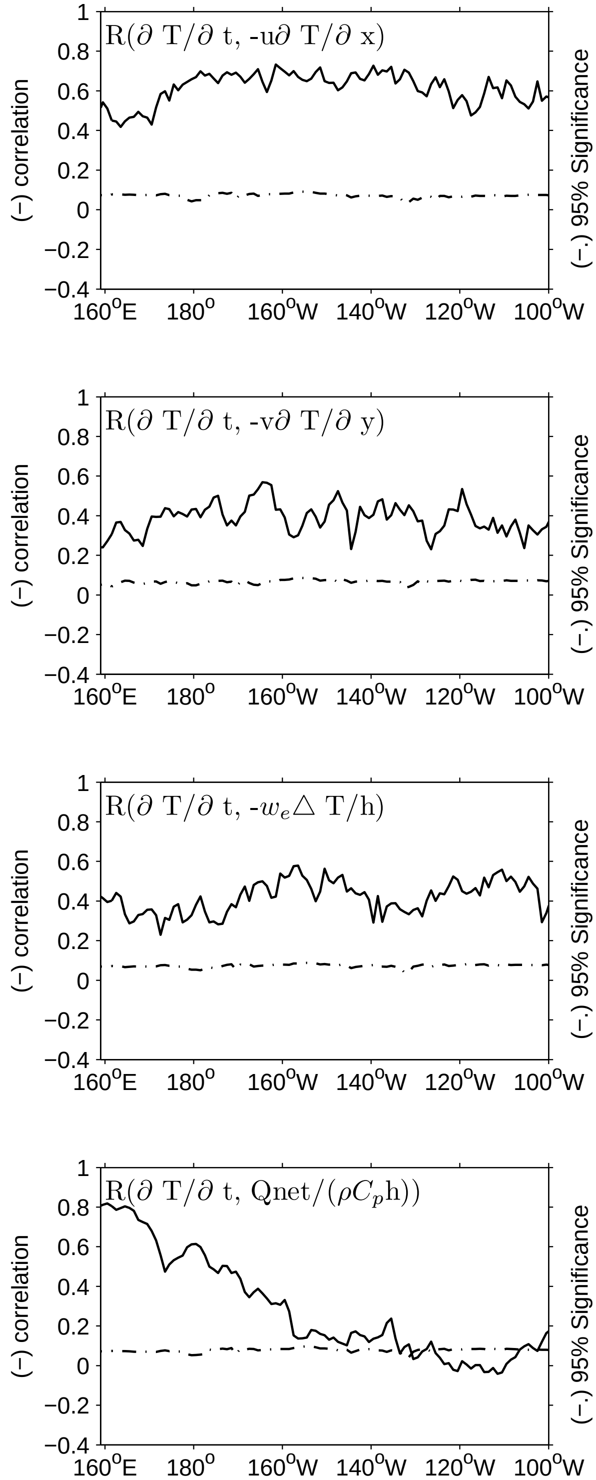

Figure 9: Same as Fig. 6 left panel, but for low-frequency signal.

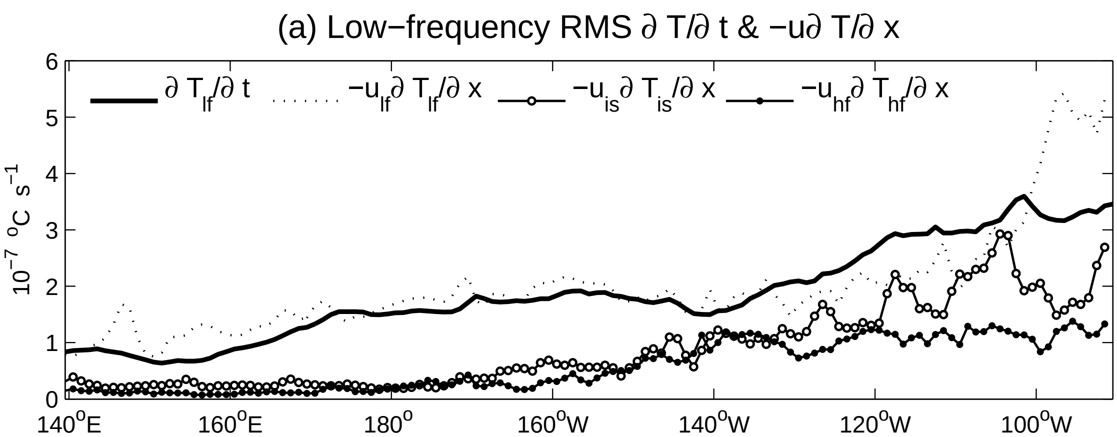

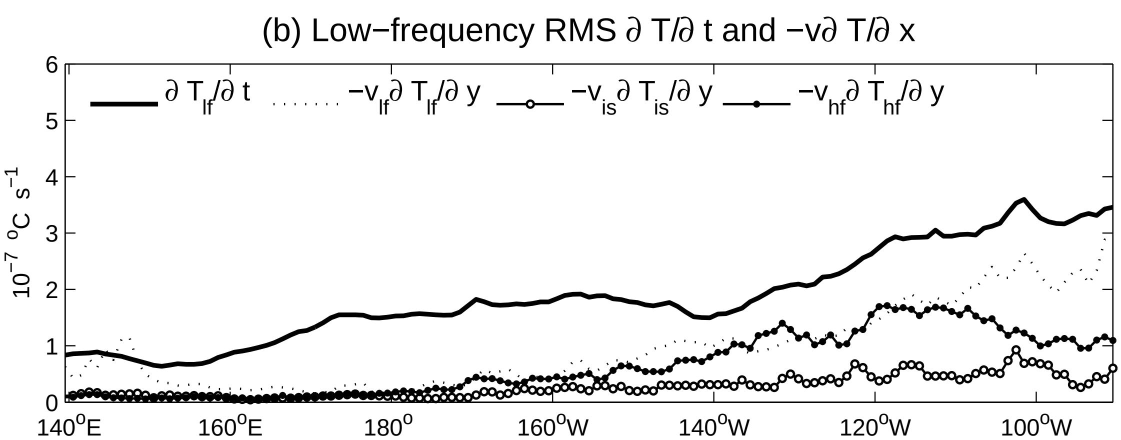

Figure 10: Same as Fig. 7, but for low-frequency signal and three largest terms.

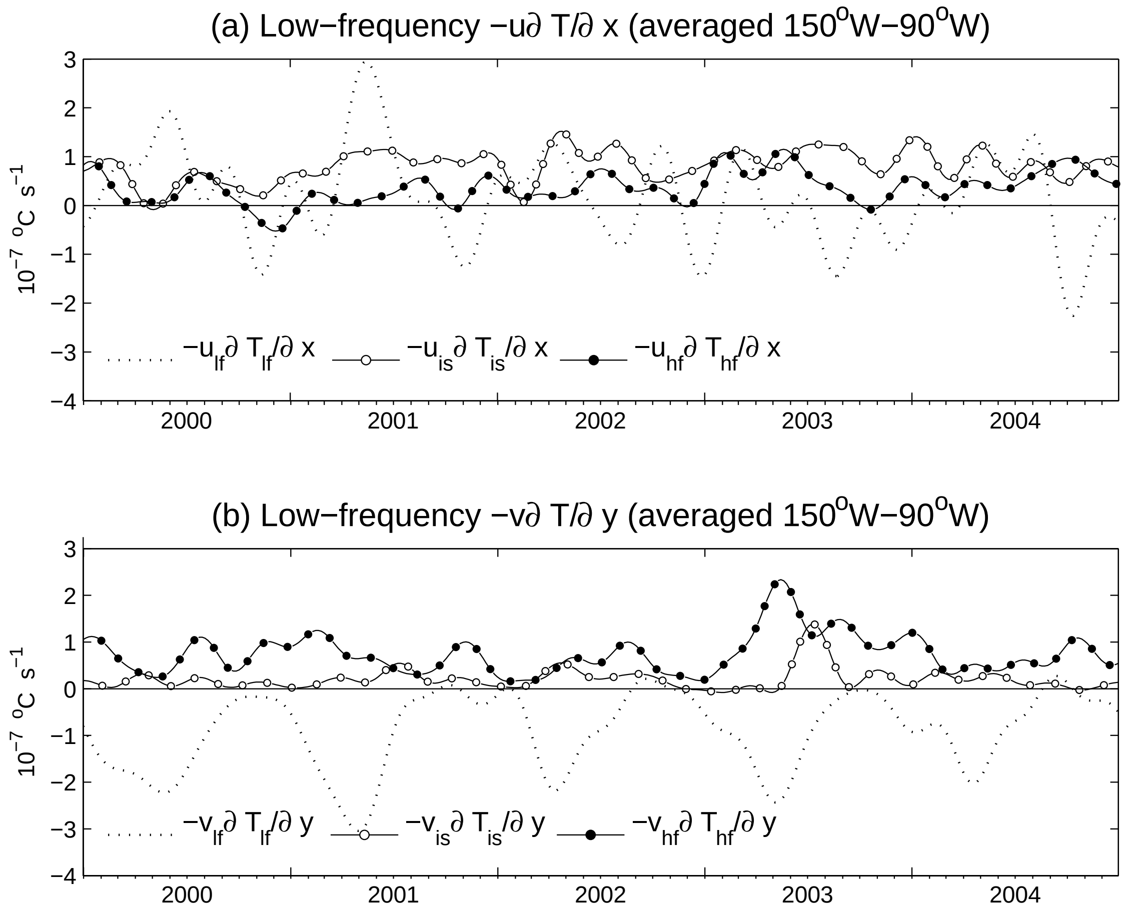

Figure 11: Time series of the largest three terms averaged from $150^oW - 90^oW$ in (a) zonal advection, and (b) the meridional advection from Jan 2000 to Dec 2004.

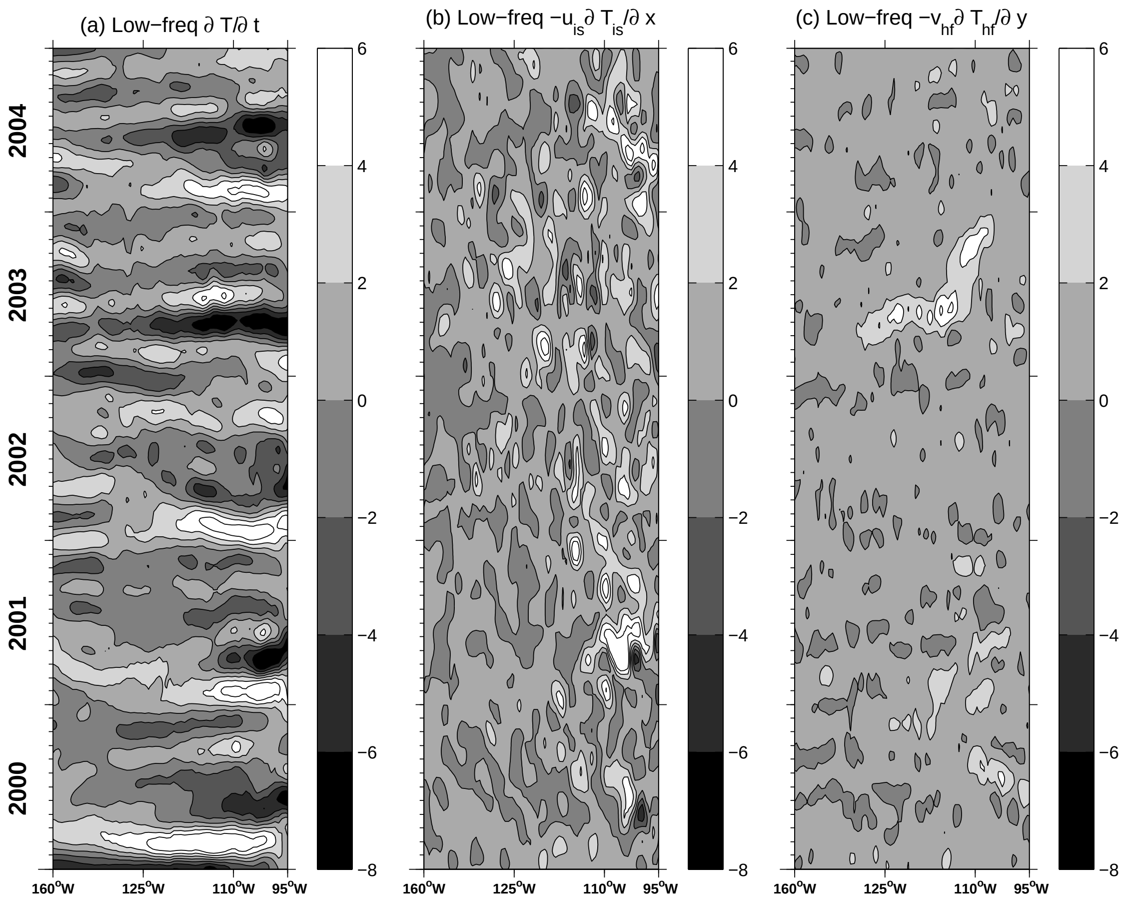

Figure 12: Time-longitude plots of the (a) low-frequency temperature tendency, (b) intra-seasonal zonal advection of the intra-seasonal zonal temperature gradient, and (c) high-frequency meridional advection of the high-frequency meridional temperature gradient. Units are $10^{-7}\ ^oCs^{-1}$.

List of Tables

Table 1: Physical interpretation of some crossterms in (2) and (3).

Crossterms	**Physical interpretation of advection terms**
(a) $-u_{lf}\frac{\partial T_{is}}{\partial x}$	zonal advection of T anomalies from Kelvin waves by low-frequency velocity
(b) $-u_{is}\frac{\partial T_{lf}}{\partial x}$	zonal advection by velocity anomalies from Kelvin waves
(c) $-u_{lf}\frac{\partial T_{lf}}{\partial x}$	low-frequency zonal advection
(d) $-u_{is}\frac{\partial T_{is}}{\partial x}$	zonal rectification from Kelvin waves
(e) $-v_{hf}\frac{\partial T_{hf}}{\partial y}$	meridional rectification from TIWs